energies

MDPI

Article

Developing a Proximate Component Prediction Model of Biomass Based on Element Analysis

Sunyong Park [1,†], Seok Jun Kim [1,†], Kwang Cheol Oh [2], La Hoon Cho [1] and DaeHyun Kim [1,3,*]

[1] Department of Interdisciplinary Program in Smart Agriculture, Kangwon National University, Hyoja 2 Dong 192-1, Chuncheon-si 24341, Republic of Korea
[2] Agriculture and Life Science Research Institute, Kangwon National University, Hyoja 2 Dong 192-1, Chuncheon-si 24341, Republic of Korea
[3] Department of Biosystems Engineering, Kangwon National University, Hyoja 2 Dong 192-1, Chuncheon-si 24341, Republic of Korea
* Correspondence: daekim@kangwon.ac.kr; Tel.: +82-33-250-6496
† These authors contributed equally to this work.

Abstract: Interest in biomass has increased due to current environmental issues, and biomass analysis is usually performed using element and proximate analyses to ascertain its fuel characteristics. Mainly, element component prediction models have been developed based on proximate analysis, yet few studies have predicted proximate components based on element analysis. Hence, this study developed a proximate component prediction model following the calorific value calculation. Analysis of Pearson's correlation coefficient showed that volatile matter (VM) and fixed carbon (FC) were positively correlated with hydrogen and oxygen, and with carbon, respectively. Thus, the model correlation was developed using a combination of the "stepwise" and "enter" methods along with linear or nonlinear regressions. The optimal models were developed for VM and ash content (Ash). The VM optimal model values were: R^2 = 0.9402, root-mean-square error (RMSE) = 7.0063, average absolute error (AAE) = 14.8170%, and average bias error (ABE) = −11.7862%. For Ash, the values were: R^2 = 0.9249, RMSE = 2.9614, AAE = 168.9028%, and ABE = 167.2849%, and for FC, the values were: R^2 = 9505, RMSE = 6.3214, AAE = 18.3199%, and ABE = 15.0094%. This study provides a model to predict the proximate component by element analysis. Contrary to existing method, proximate analysis can be predicted based on elemental analysis, and shows that consume samples can be performed at once.

Keywords: proximate analysis; element analysis; prediction model; biomass

Citation: Park, S.; Kim, S.J.; Oh, K.C.; Cho, L.H.; Kim, D. Developing a Proximate Component Prediction Model of Biomass Based on Element Analysis. *Energies* **2023**, *16*, 509. https://doi.org/10.3390/en16010509

Academic Editor: Alok Kumar Patel

Received: 29 November 2022
Revised: 19 December 2022
Accepted: 27 December 2022
Published: 2 January 2023

1. Introduction

Interest in environmental issues and climate change has increased globally, leading to an increased interest in using biomass rather than fossil fuels such as coal. Various technologies such as torrefaction and pyrolysis have been suggested for the use of solid biomass. Particularly, there is increasing interest in biochar, which is inherently important in terms of response to climate change, soil improvement, energy production, and waste management. Evaluation of fuel characteristics is important for methods to use as a solid energy source, such as biochar or torrefaction. To analyze the fuel characteristics of solid biomass, element and proximate analyses should be performed. The amount of element composition of carbon (C), hydrogen (H), nitrogen (N), sulfur (S), and oxygen (O) can be ascertained by element analysis. The amount of moisture content (MC), volatile matter (VM), fixed carbon (FC), and ash content (Ash) can be analyzed by proximate analysis. Additionally, the predicted calorific value based on element or proximate analyses has been suggested; however, these analyses are expensive and time-consuming. Various studies have been conducted to solve the problems as follows: the elemental composition derived through proximate analysis was confirmed [1–3]; the prediction of elemental

composition was developed using proximate analysis in the biomass ranges of 4.7% ≤ FC ≤ 38.4%, 57.2% ≤ VM ≤ 90.6%, 36.2% ≤ C ≤ 53.1%, 4.36% ≤ H ≤ 8.3%, and 31.37% ≤ O ≤ 49.5% [4]; the prediction model of higher heating value (HHV) was suggested using element and proximate analysis of biochar [5]; and conventional prediction models of HHV were compared and a developed prediction model was suggested [6]. Recently, a method of predicting using artificial intelligence (AI) has been proposed. The prediction of elemental composition was developed using proximate analysis via AI models such as artificial neural network (ANN), adaptive neuro-fuzzy inference system (ANFIS), and multilinear regression (MLR) [7]. The above-mentioned studies predicted elemental composition either by using proximate analysis alone or by predicting the heating value using element or proximate analyses. However, as the earlier studies predicted elemental analysis based on proximate analysis, very few studies have been conducted on the prediction of proximate analysis using element analysis, which is the main objective of this study. Additionally, using the result of the predicted proximate analysis, this study further predicts the calorific value for verification. Through this, it was considered that fuel characteristic analysis such as fuel ratio, which can be confirmed through proximate analysis only through elemental analysis, could be confirmed.

2. Materials and Methods

2.1. Collection and Selection of Suitable Data

A total of 299 element and proximate analyses data sets were collected from previous research. The collected 244 element and proximate analyses results were used to derive correlations [2–4,6–47], and thereafter, 55 data sets were obtained for correlation validation (Table 1). The data for correlations derivation and validation are summarized in Table S1 and Table 1. For calorific value, 149 data sets were used for prediction and validation. The linear and nonlinear regressions were performed on the ultimate analysis data using IBM SPSS 22.0 to obtain correlation equations with different goodness of fit. The data fitting and analysis in this study combined the "stepwise" and "enter" methods in SPSS software.

2.2. Element and Proximate Analyses

In this study, untreated pepper stem and samples of torrefied pepper stems at 200, 230, and 270 °C for 20, 30, and 40 min were analyzed. Based on the quality test method for solid fuel products stipulated by the Ministry of Environment in Korea [48], elemental analysis was conducted to determine the contents of the elements C, H, N, and S (FlashEA 1112, Thermo Fisher Scientific, MA, USA). The oxygen content was calculated as follows.

$$O\ [\%] = 100 - (C + H + N + S) \quad (1)$$

Proximate analysis of the selected biomass samples was conducted following ISO standards protocols for moisture content [49], VM [50], and Ash [51].

Table 1. Data set for correlation validation (n = 55).

C [%]	H [%]	N [%]	O [%]	S [%]	VM [%]	FC [%]	Ash [%]	Ref
44.414	6.07	0.977	40.2	0	76	9.05	3.55	This study
45.241	5.514	0.858	31.007	0	75.1	13.09	3.61	
45.533	5.603	0.989	30.269	0	74.21	14.48	3.91	
45.222	5.928	1.001	30.132	0	73.9	15.73	6.61	
48.417	5.841	1.008	29.208	0	73.25	16.51	3.6	
50.262	5.549	1.034	30.726	0	72.27	18.42	3.68	
50.629	5.533	1.098	27.841	0	72.03	19.15	3.56	
54.011	5.501	1.08	24.995	0	67.9	23.6	3.98	
54.954	5.738	1.218	25.817	0	65.56	25.92	4.2	
55.038	5.492	0.927	25.474	0	65.36	26.53	3.96	

Table 1. *Cont.*

C [%]	H [%]	N [%]	O [%]	S [%]	VM [%]	FC [%]	Ash [%]	Ref
43.25	5.57	0.6	41.89	0	73.87	17.44	8.69	[52]
48.18	5.46	0.69	36.2	0	71.53	19	9.47	
55.03	4.97	0.82	28.63	0	62.59	26.86	10.55	
61.7	4.19	0.94	21.88	0	45.45	43.26	11.29	
59.980	5.400	0.250	33.350	0	66.47	28.55	0.98	[53]
60.980	5.100	0.210	32.690	0	62.85	32.36	0.98	
63.440	5.100	0.180	30.720	0	65.71	30.24	0.54	
64.370	5.000	0.180	29.800	0	65.71	30.24	0.65	
51.910	6.100	0.100	41.000	0	69.80	18.20	0.74	
50.300	5.300	0.000	44.400	0	84.20	15.50	0.30	[54]
51.700	5.400	0.000	42.900	0	80.60	19.20	0.35	
54.400	5.200	0.000	40.400	0	75.70	24.20	0.40	
47.000	6.070	0.210	46.600	0.120	82.94	16.14	0.92	[55]
47.920	3.500	1.340	47.060	0.170	30.56	43.17	26.27	
58.430	3.010	1.020	37.380	0.160	20.82	57.19	21.99	
67.310	2.670	0.870	28.980	0.170	5.33	77.35	17.32	
74.080	2.500	0.500	22.740	0.170	4.72	83.25	12.03	
62.200	5.180	1.690	24.210	0	60.77	32.50	6.72	[56]
71.130	4.030	1.940	15.050	0	29.85	62.30	7.85	
74.880	2.880	1.770	10.410	0	23.19	66.75	10.06	
80.010	2.720	1.280	6.590	0	14.86	75.73	9.40	
45.150	5.150	0.750	42.920	0.140	75.55	18.58	5.87	[57]
71.340	3.930	1.430	10.840	0.240	27.06	62.72	12.22	
75.030	2.620	1.410	7.790	0.240	17.49	69.60	12.91	
78.480	1.880	1.530	3.940	0.320	11.49	74.66	13.85	
44.430	6.160	0.180	49.230	0	67.30	19.50	1.70	[58]
45.710	5.890	0.000	48.400	0	69.60	18.80	0.90	
79.970	3.530	0.010	16.490	0	32.10	60.00	3.10	
79.820	3.550	0.010	16.620	0	29.20	61.30	4.80	
77.480	3.640	0.100	18.780	0	25.00	69.10	2.00	
78.190	3.220	0.690	17.900	0	27.60	66.80	2.80	
76.950	3.320	0.740	18.899	0	26.10	68.10	1.00	
78.540	3.250	0.590	17.620	0	25.00	71.30	1.00	
46.370	6.290	46.790	0.550	0.110	83.46	14.26	2.17	[59]
41.920	4.210	53.640	0.230	0.100	71.18	26.94	1.77	
47.160	4.730	47.850	0.250	0.130	71.86	25.52	2.49	
52.700	3.800	43.220	0.280	0.140	62.19	34.46	3.22	
58.250	2.810	38.680	0.310	0.150	51.85	44.04	3.95	
45.650	5.120	39.630	1.660	0.920	73.94	14.39	7.020	[60]
58.040	4.280	18.790	2.750	0.870	43.82	37.21	15.270	
59.140	3.470	14.540	2.530	0.790	31.78	42.38	19.530	
62.590	3.360	9.910	2.510	0.770	21.12	51.78	20.860	
63.930	0.670	9.430	2.150	0.860	18.73	54.11	20.960	
63.830	1.650	9.330	2.110	0.630	17.83	54.07	22.390	
62.010	1.850	9.790	2.220	0.670	17.50	54.01	23.460	

2.3. Evaluation of Correlations

Pearson correlation was used to ascertain the correlation between each element (C, H, N, O, S) and the proximate analysis results (VM, FC, Ash). The degree of correlation between two populations can be analyzed using the Pearson correlation coefficient, which is expressed in Equation (2). The range of correlation through analysis is from −1 to 1. Positive or negative correlations were analyzed as proportional or inverse relationships,

respectively. The closer the values were to −1 or 1, the more linear the correlation was; the closer the values were to 0, the lower the correlation in the relationship [61]. The correlation can be explained as the best-fitted regression line if the estimation error tends to be zero [62]. However, the low estimated error values could not indicate the high correlation completely. For choosing the most appropriate correlation equation, the average absolute error (AAE) and average bias error (ABE) were evaluated to select the best correlation [5]. AAE and ABE were expressed as shown in Equations (3) and (4). The coefficient of determination value (R^2) was calculated as shown in Equation (5) to determine the degree of goodness of the proposed correlation [46,63,64].

$$R = \frac{\left(\sum_{i=1}^{n}\left(X_i - \overline{X}\right)\left(Y_i - \overline{Y}\right)\right)}{\sqrt{\sum_{i=1}^{n}\left(X_i - \overline{X}\right)^2}\sqrt{\sum_{i=1}^{n}\left(Y_i - \overline{Y}\right)^2}} \quad (2)$$

$$AAE = \frac{1}{n}\sum_{i=1}^{n}\left|\frac{Value_p - Value_M}{Value_M}\right|, \quad (3)$$

$$ABE = \frac{1}{n}\sum_{i=1}^{n}\left[\frac{Value_p - Value_M}{Value_M}\right], \quad (4)$$

$$R^2 = 1 - \frac{\sum_{i=1}^{n} Value_m - Value_P}{\sum_{i=1}^{n} Value_m - \overline{Value_P}}. \quad (5)$$

The AAE basically quantified the proximity of the predicted to the experimental value such as VM, FC, Ash, and HHV, with the lower AAE indicating a higher accuracy of the specific correlation. The positive ABE value implied that the average predicted value of VM, FC, Ash, and HHV was higher than the measured value. The smaller the absolute value of the ABE, the smaller the deviation of correlation. Considering that the correlation of each element was a nonlinear relationship, the square or square root was also considered for correlation.

2.4. Prediction of HHV

For predicting HHV, the Equation (6) by Ref. [5] was followed. The measured HHV was compared with that of the calculated using the proximate analysis results. Thereafter, HHV was calculated using derived optimal model of VM, FC, and Ash, and was compared with that of the measured HHV. The stepwise progression of this study is summarized in Figure 1.

$$HHV = 36.5FC + 18.8VM - 2.1Ash, \quad (6)$$

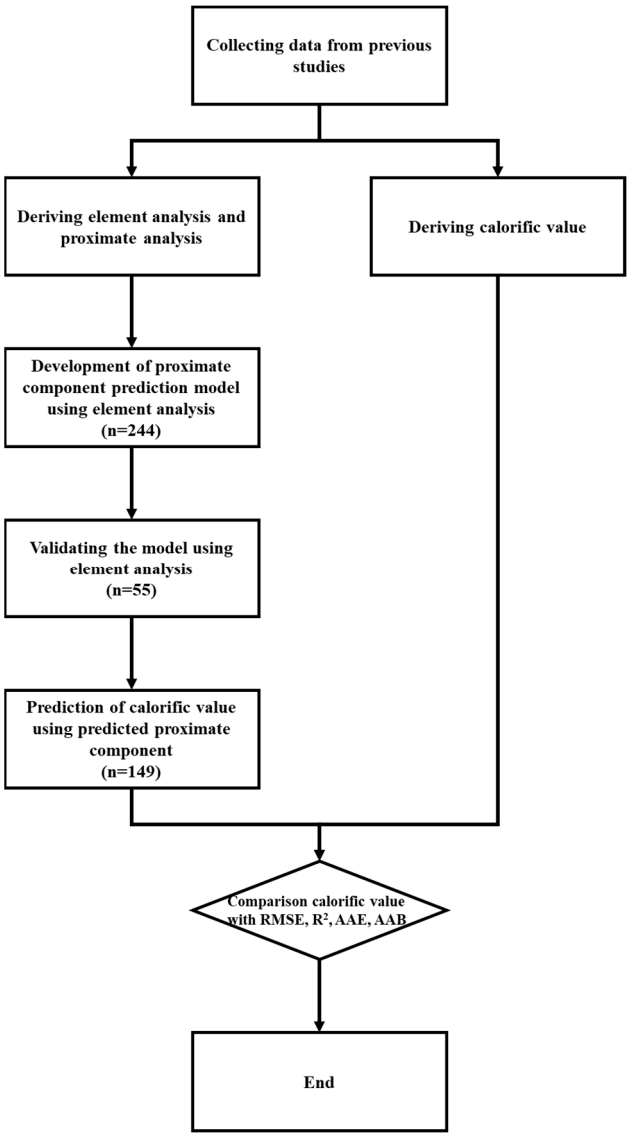

Figure 1. Flow chart depicting the stepwise progression of this study.

3. Results & Discussions

3.1. Pearson Correlation

The Pearson correlation is shown in Table 2. Through the Pearson correlation, the correlation between the element and proximate components was ascertained. VM showed a significantly positive correlation with H and O, but had a strong negative correlation with C. However, C was significantly positively correlated with FC. Ash was correlated with H, N, and O, but it was not as strong when compared to FC and VM with H, O, and C.

3.2. Prediction Equation of VM

The prediction results were based on elemental data of various kinds of biomass, including C, H, N, O, and S. The analytical data used in the independent variable range was $34.02 \leq C \leq 90.68$, $0.5 \leq H \leq 8.21$, $3.43 \leq O \leq 57.2$, $0 \leq N \leq 7.92$, and $0 \leq S \leq 1.38$. As presented in Table 3, for one-dimensional equations, the equation using H had the highest correlation, which was due to the high correlation between H and VM. The equation using the square of H and O showed a lower correlation than that of the first-order equation. Although in C, a slight increase in correlation was observed. Optimal fitness correlation in linear regression is as in Equation (C9). In nonlinear regression, the overall correlation of the resulting equation was higher than that obtained by linear analysis. Equation (C13)

gave the best prediction, with R^2, RMSE, AAE, and ABE as 0.9250, 6.66, 15.7622, and 0.3097, respectively.

Table 2. Result of Pearson correlation between C, H, N, O, S, VM, FC, and Ash.

	C	**H**	**N**	**O**	**S**	**VM**	**FC**	**Ash**
C	1	−0.5505 **	0.1434 *	−0.7256 **	0.0318	−0.7053 **	0.8622 **	−0.0253
H	−0.5505 **	1	−0.2842 **	0.6765 **	0.0215	0.8966 **	−0.8243 **	−0.5461 **
N	0.1434 *	**−0.2842 ** **	1	**−0.2536 ** **	**0.2917 ** **	**−0.3554 ** **	**0.2596 ** **	**0.3108 ** **
O	**−0.7256 ** **	**0.6765** **	**−0.2536 ** **	1	**−0.1745 ** **	**0.8159 ** **	**−0.7708 ** **	**−0.4648 ** **
S	0.0318	0.0215	**0.2917 ** **	**−0.1745 ** **	1	−0.0279	0.0043	0.0382
VM	**−0.7053 ** **	**0.8966 ** **	**−0.3554 ** **	**0.8159 ** **	−0.0279	1	**−0.9222 ** **	**−0.5928 ** **
FC	**0.8622 ** **	**−0.8243 ** **	**0.2596 ** **	**−0.7708 ** **	0.0043	**−0.9222 ** **	1	0.2596 **
Ash	−0.0253	**−0.5461 ** **	**0.3108 ** **	**−0.4648 ** **	0.0382	**−0.5928 ** **	**0.2596 ** **	1

**: The correlation is significant at the 0.01 level (both sides). *: The correlation is significant at the 0.05 level (both sides).

Table 3. Correlations used for predicting the VM of biomass based on element analysis.

Sr. No.	**Equation**	**R^2 [-]**	**RMSE [-]**	**AAE [%]**	**ABE [%]**
(C1)	$VM = 127.462 - 1.333C$	0.4974	17.0704	54.4482	34.1155
(C2)	$VM = -12.186 + 13.461H$	0.8038	10.6537	25.3121	5.9353
(C3)	$VM = 13.802 + 1.239O$	0.6657	14.4275	50.6227	33.4789
(C4)	$VM = 87.763 - 0.011C^2$	0.4975	17.0928	54.6742	30.1169
(C5)	$VM = 12.983 + 1.54H^2$	0.7691	11.5869	27.1061	12.6207
(C6)	$VM = 42.716 + 0.008O^2$	0.6256	19.7179	74.6681	48.2968
(C7)	$VM = 18.811 - 0.412C + 9.716H + 0.323O$	0.8930	7.9366	20.3251	5.9650
(C8)	$VM = 23.219 - 0.438C + 9.618H + 0.289O - 1.292N$	0.9000	7.6557	19.3833	4.8161
(C9)	$VM = 13.647 - 0.344C + 8.902H + 0.547O - 2.02N + 3.945S$	0.9067	7.3231	19.4227	3.0326
(C10)	$VM = 36.348 - 0.005C^2 + 1.165H^2 + 0.002O^2$	0.8587	9.1222	22.7587	8.3646
(C11)	$VM = 37.389 - 0.005C^2 + 1.163H^2 + 0.01O^2 - 0.272N^2$	0.8834	12.7811	29.5636	25.5124
(C12)	$VM = 94.085 + 71.641H + 1.779O - 0.004C^2 - 2.896H^2 - 0.007O^2 + 2.775C^{0.5} - 146.244H^{0.5} - 9.57O^{0.5}$	0.9175	6.9817	16.2266	5.2507
(C13)	$VM = 100.873 + 71.894H + 1.569O - 0.005C^2 - 2.891H^2 - 0.006O^2 + 2.965C^{0.5} - 147.959H^{0.5} - 8.662O^{0.5} + 1.54N + 0.031N^2 - 5.932N^{0.5}$	0.9250	6.6600	15.7622	0.3097
(C14)	$VM = 14.649 + 36.404H^{0.5} - 0.003C^2 - 5.644N^{0.5} + 3.738O - 22.538O^{0.5} + 0.862N^2 - 0.019O^2$	0.8529	9.2252	28.407	10.3855

3.3. Prediction Equation for Fixed Carbon

Table 4 summarizes fixed carbon prediction equations. For the one-dimensional equations, those using C had the highest correlation, which was due to the high correlation between C and FC. This trend was similarly observed for the squared or 0.5-squared of each element. Unlike VM, FC showed a relatively high correlation in a linear equation. Compared with the one-dimensional equation (Equations (C15)–(C20)), Equations (C21) and (C22) showed an increased improvement in correlation. Optimal fitness correlation in linear regression was selected as shown in Equation (C23). For the nonlinear regression, the overall correlation of the resulting equation was higher than that obtained by linear analysis. Equation (C28) gave the best prediction, showing R^2, RMSE, AAE, and ABE as 0.9268, 5.62353, 18.9730, and 9.4295, respectively. Compared with Equations (C23) and (C28), a good correlation was observed in Equation (C28), although lower ABE was observed in Equation (23). Hence, both the models (Equations (C23) and (C28)) were selected as optimal.

Table 4. Correlations used for predicting the FC of biomass based on element analysis.

Sr. No.	Equation	R^2 [-]	RMSE [-]	AAE [%]	ABE [%]
(C15)	$FC = -44.34 + 1.419C$	0.7433	10.4127	31.8162	11.3907
(C16)	$FC = 86.126 - 10.748H$	0.6795	11.3906	36.4873	15.7797
(C17)	$FC = 72.757 - 1.214O$	0.5941	12.9860	33.5692	14.5535
(C18)	$FC = -2.037 + 0.011C^2$	0.7421	10.7255	30.2706	10.2721
(C19)	$FC = 66.737 - 1.259H^2$	0.6443	11.9632	40.5426	16.3633
(C20)	$FC = 58.372 - 0.021O^2$	0.5670	13.3558	37.6647	11.3571
(C21)	$FC = 16.459 + 0.919C - 6.805H - 0.007O$	0.9171	5.9237	19.5598	5.3955
(C22)	$FC = 13.801 + 0.931C - 6.666H + 0.008O + 0.808N$	0.9180	5.8812	19.6145	5.3913
(C23)	$FC = 8.714 + 1.029C - 6.273H + 0.04O + 0.624N - 1.413S$	0.9204	5.7581	19.2783	4.6649
(C24)	$FC = 35.479 + 0.007C^2 - 0.737H^2 - 0.003O^2$	0.9016	6.4338	22.3712	9.9211
(C25)	$FC = 34.019 + 0.007C^2 - 0.719H^2 - 0.003O^2 + 0.221N^2$	0.9054	6.2763	21.5914	8.1136
(C26)	$FC = -23.481 + 14.992C^{0.5} - 26.012H^{0.5} + 0.527O^{0.5}$	0.9104	6.1652	20.0298	5.3331
(C27)	$FC = 37.854 + 0.964C - 26.536H + 0.288N^2$	0.9115	6.0648	19.5750	5.9540
(C28)	$FC = -19.694 + 0.009C - 48.623H + 2.035H^2 + 97.102H^{0.5} + 0.252N^2 - 2.151N^{0.5} + 2.471S^{0.5}$	0.9268	5.6253	18.9730	9.4295

3.4. Prediction Equation for Ash Content

The prediction equation for Ash had the lowest correlation compared with VM and FC, which was likely because the components of Ash were few in C, H, N, O, and S as shown by elemental analysis. The correlation used for predicting the Ash is summarized in Table 5. In the linear regression model, Equations (C31) and (C32) showed high R^2 and low RMSE values, which were R^2 of 0.6484 and 0.6560 and RMSEs of 5.3865 and 5.2976, respectively. In the nonlinear regression model, most of the models had an R^2 value over 0.6 except for Equation (34). Among them, Equation (39) showed the highest R^2 (0.6728) and lowest RMSE (5.1776). Compared to the linear regression model in Equations (C31) and (32) and the nonlinear regression model in Equation (C39), the correlation and RMSE of Equation (C39) were higher, while AAE and ABE were lower, respectively. Therefore, Equations (C31) and (C32) were selected as the optimal models.

Table 5. Correlations used for predicting the Ash of biomass based on element analysis.

Sr. No.	Equation	R^2 [-]	RMSE [-]	AAE [%]	ABE [%]
(C29)	$Ash = 28.877 - 3.37H$	0.2982	7.9190	303.3270	285.9455
(C30)	$Ash = 23.709 - 2.277H - 0.113O + 1.144N$	0.3380	7.3494	194.8745	167.9517
(C31)	$Ash = 74.551 - 0.653C - 2.853H - 0.5O + 0.802N$	0.6484	5.3865	103.6460	76.8950
(C32)	$Ash = 75.431 - 0.653C - 2.683H - 0.529O + 0.995N - 3.063S$	0.6560	5.2976	125.2741	102.4342
(C33)	$Ash = 60.279 - 4.418H - 3.83C^{0.5}$	0.4299	6.8310	221.2780	191.7969
(C34)	$Ash = 112.918 - 2.756H - 8.323C^{0.5} - 5.011O^{0.5}$	0.6052	5.6840	157.2964	135.5372
(C35)	$Ash = 94.342 - 8.242H - 8.325C^{0.5} - 4.973O^{0.5} + 20.801H^{0.5}$	0.6077	5.6679	148.8836	124.5218
(C36)	$Ash = 46.519 - 44.925H - 8.343C^{0.5} - 4.771O^{0.5} + 102.495H^{0.5} + 1.85H^2$	0.6442	5.4023	152.1289	131.2397
(C37)	$Ash = 42.152 - 44.323H - 8.16C^{0.5} - 4.586O^{0.5} + 101.844H^{0.5} + 1.817H^2 + 1.681N^{0.5}$	0.6672	5.2237	129.8906	109.7289
(C38)	$Ash = 50.852 - 39.585H - 8.445C^{0.5} - 4.9O^{0.5} + 91.971H^{0.5} + 1.572H^2 + 2.325N^{0.5} - 3.252S^{0.5}$	0.6728	5.1776	130.2347	109.3955
(C39)	$Ash = 53.468 - 10.279S^{0.5} + 5.688S - 0.306N^2 - 2.638H + 2.309N - 0.521O - 0.004C^2$	0.6527	5.6506	174.3943	157.5633

3.5. Validation of Correlation Equation

To verify the availability of the correlation equations, the data in some studies that measured the biomass were selected and tested shown in Table 6 and Figure 2. For VM, Equations (C9) and (C13) showed higher R^2. Equation (C9) showed a lower RMSE than the model, and Equation (C13) showed a higher RMSE. The AAE and ABE of each equation was 14.8170 and −11.7862, and 17.9723 and −15.9829, respectively. Equation (C9) showed fewer errors than Equation C13. Hence, Equation (9) was selected as the optimal model. Comparing Equations (C23) and (C28) for FC, Equation (C28) showed a well-fitted correlation, with an R^2 of 0.9585. Moreover, Equation C23 had a lower RMSE of 6.3214, while Equation C28 showed 6.3810. A comparison between Equations (C23) and (C28) in terms of AAE and ABE showed that Equation (C23) was higher in AAE but lower in ABE. Therefore, both models (Equations (C23) and (C28)) were selected as optimal. For the validation of Ash, Equation (C32) was shown to be a better-fitting model; however, the RMSE, AAE, and AAE values showed that Equation C31 was more optimal.

Table 6. Summary of validation results of VM, FC, and Ash.

		R^2 [-]	RMSE [-]	AAE [%]	ABE [%]
VM	Equation (C9)	0.9402	7.0063	14.8170	−11.7862
	Equation (C13)	0.9476	6.8838	17.9723	−15.9829
FC	Equation (C23)	0.9505	6.3214	18.3199	15.0094
	Equation (C28)	0.9582	6.3810	17.7130	16.1190
Ash	Equation (C31)	0.9249	2.9614	168.9028	167.2849
	Equation (C32)	0.9326	3.0426	202.5436	201.9132

3.6. Prediction of HHV

The measured HHV were compared with that of the calculated values using measured proximate analysis, and the result comparing the measured and calculated HHVs by measured proximate component was named as "Measured." R^2, RMSE, AAE, and ABE of Measured were observed as 0.7733, 2.1876, 8.6677, and 4.1273, respectively. Additionally, predicted VM, FC, and Ash calculated from the optimal model were used for calculating HHV. The combinations of models are summarized in Table 7, showing a total of 8 combinations. Table 8 showed the result of HHV prediction. All combinations were shown to have better correlation than that of those measured, although Comb_5 and Comb_6 showed lower RMSE, AAE, and ABE than the other combinations: RMSE 1.9382 and 1.9356, AAE 7.4788 and 7.4612, and ABE 4.3765 and 4.3413, respectively. Figure 3 showed scatter plots showing the comparison between predicted and experimental HHV of each combination.

Table 7. Summarization of each combination model for prediction of HHV.

	Measured	VM		FC		Ash	
		Equation (C9)	Equation (C13)	Equation (C23)	Equation (C28)	Equation (C31)	Equation (C32)
Measured	√	-	-	-	-	-	-
Comb_1	-	√	-	√	-	√	-
Comb_2	-	√	-	-	√	-	√
Comb_3	-	-	√	√	-	√	-
Comb_4	-	-	√	-	√	-	√
Comb_5	-	√	-	√	-	√	-
Comb_6	-	√	-	-	√	-	√
Comb_7	-	-	√	√	-	√	-
Comb_8	-	-	√	-	√	-	√

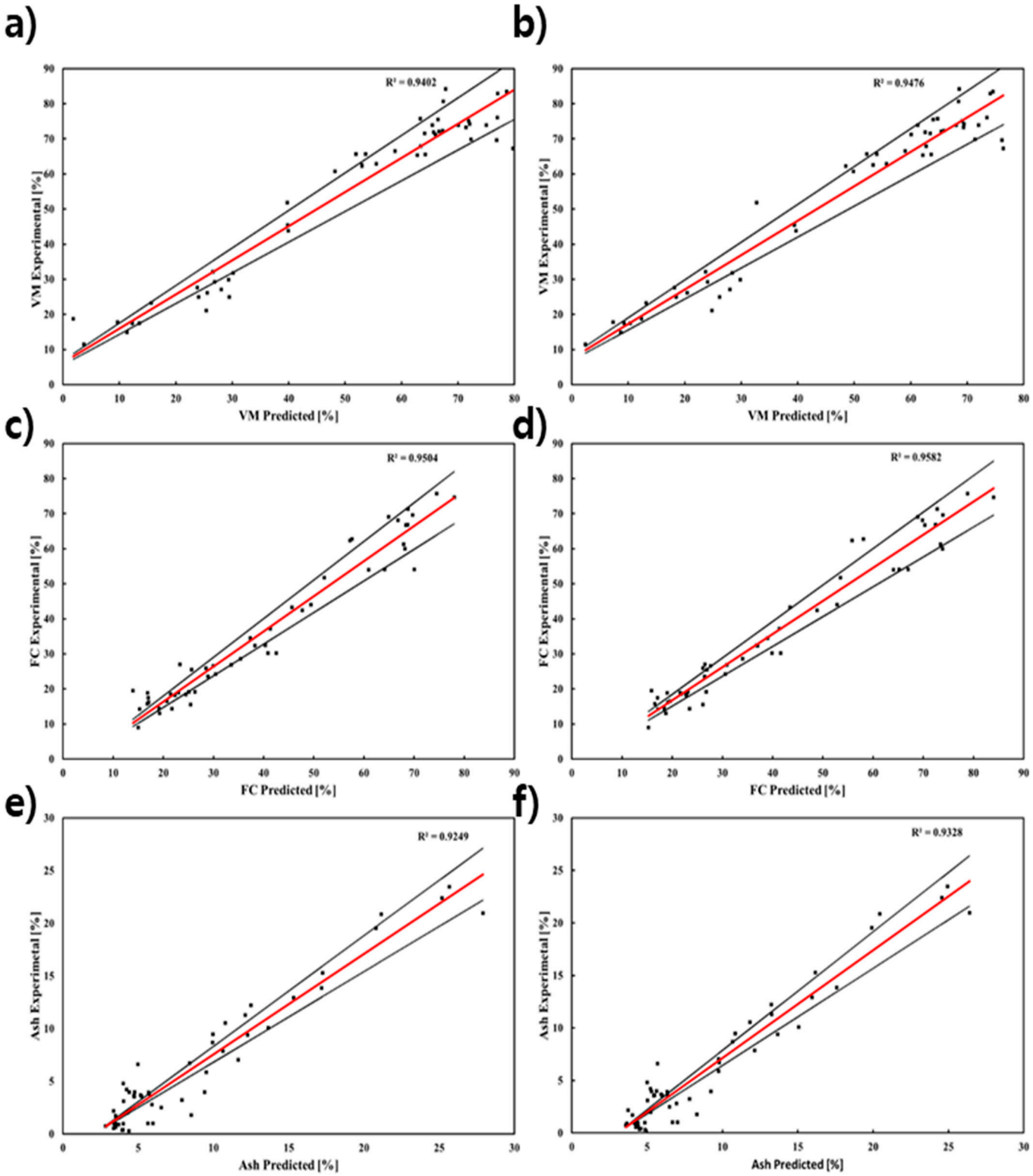

Figure 2. Scatter plots depicting the validation result of each model: (**a**) Equation (C9), (**b**) Equation (C13), (**c**) Equation (C23), (**d**) Equation (C28), (**e**) Equation (C31), and (**f**) Equation (C32).

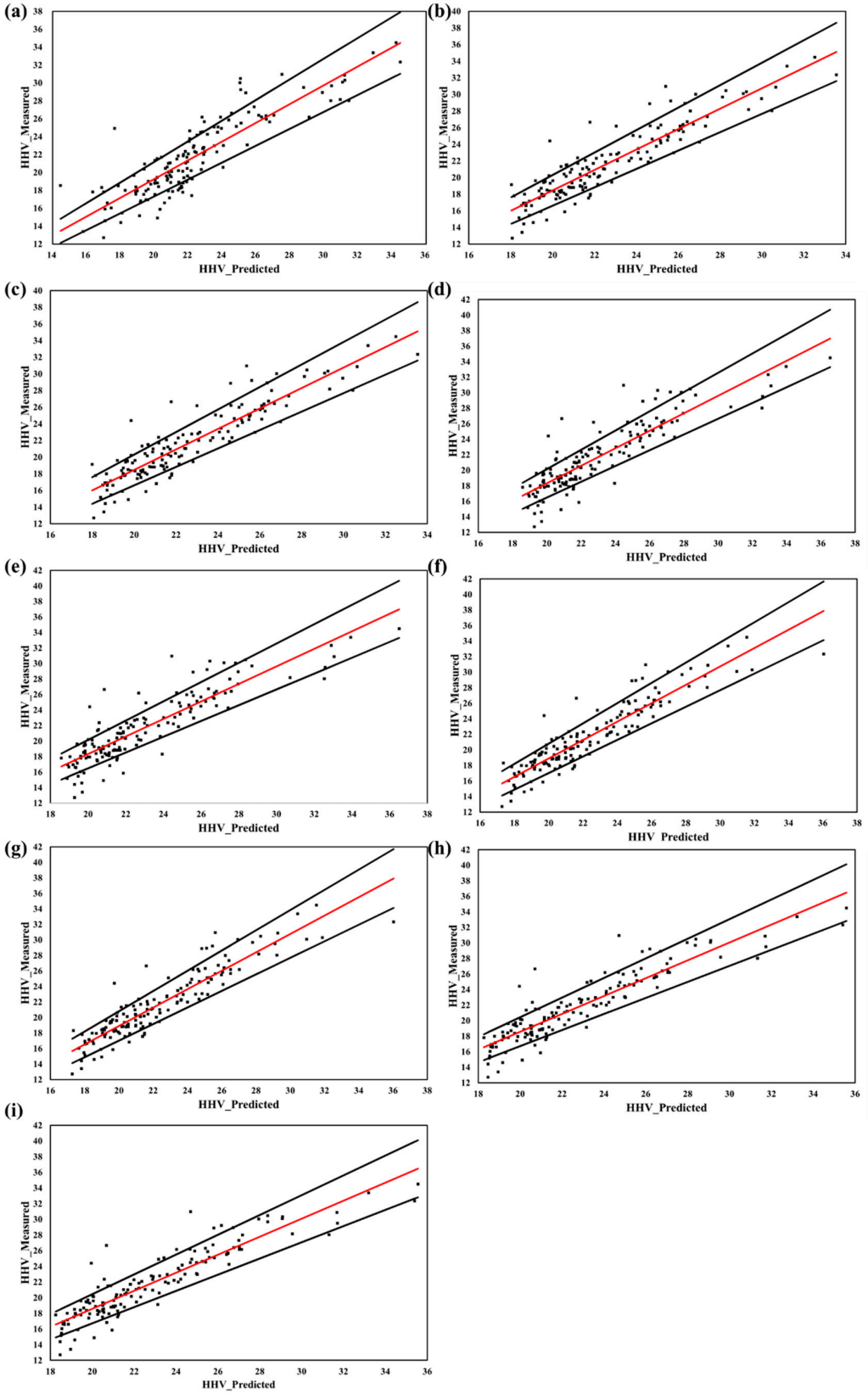

Figure 3. Scatter plots showing the comparison between predicted and experimental HHV for the (**a**) Measured, (**b**) Comb_1, (**c**) Comb_2, (**d**) Comb_3, (**e**) Comb_4, (**f**) Comb_5, (**g**) Comb_6, (**h**) Comb_7, and (**i**) Comb_8. * The black line implies ± 10% error band line.

Table 8. Summary of HHV prediction results.

	R^2 [-]	RMSE [-]	AAE [%]	ABE [%]
Measured	0.7733	2.1876	8.6677	4.1273
Comb_1	0.8369	2.1455	8.6944	5.8966
Comb_2	0.8369	2.1433	8.6834	5.8615
Comb_3	0.7805	2.4764	10.1171	7.6254
Comb_4	0.7803	2.4734	10.0993	7.5902
Comb_5	0.8485	1.9382	7.4788	4.3765
Comb_6	0.8488	1.9356	7.4612	4.3413
Comb_7	0.8343	2.1223	8.5481	6.1052
Comb_8	0.8345	2.1186	8.5293	6.0701

4. Conclusions

In this study, contrary to the method of predicting elemental analysis through proximate analysis, which was widely conducted in the past, this study attempted to predict proximate analysis results based on that of the elemental analysis. Additionally, calorific value was predicted using the result of predicted proximate composition for verifying the result of proximate composition ratio. From previous studies, a total of 299 data were collected, 244 of which were used for model production, and 55 data which were used for verification. Based on the data, the Pearson's correlations of several elements and the proximate analysis component were ascertained. VM and FC showed strongly significant positive correlations with O and H, and with C, respectively. Based on these, prediction models for VM, FC, and Ash were developed. Furthermore, the calorific value was predicted using the HHV prediction model. Various models have been suggested to predict VM, FC, and Ash, and optimal models for each component were determined as follows:

$$\mathrm{VM} = 13.647 - 0.344\mathrm{C} + 8.902\mathrm{H} + 0.547\mathrm{O} - 2.02\mathrm{N} + 3.945\mathrm{S} \quad (\text{VM model})$$

$$\mathrm{FC} = 8.714 + 1.029\mathrm{C} - 6.273\mathrm{H} + 0.04\mathrm{O} + 0.624\mathrm{N} - 1.413\mathrm{S} \quad (\text{FC model})$$

$$\mathrm{Ash} = 75.431 - 0.653\mathrm{C} - 2.683\mathrm{H} - 0.529\mathrm{O} + 0.995\mathrm{N} - 3.063\mathrm{S} \quad (\text{Ash model})$$

VM showed an RMSE, AAE, and ABE of 7.0063, 14.8170%, and −11.7862%, respectively. FC and Ash showed an RMSE, AAE, and ABE of 6.3214, 18.3199%, and 15.0094%, 2.9614, 168.9028%, and 168.2849%, respectively. Especially, the AAE and ABE of Ash were higher than 168%. It was determined that the main component of Ash did not comprise C, H, N, O, and S. Comb_5 and Comb_6 should be used for predicting HHV based on the predicted proximate component due to their low RMSE, AAE, ABE and high R^2. Overall, this study provides a method of predicting proximate analysis using only element analysis results. Through this, it is considered that time and resource consumption can be reduced by predicting proximate analysis only with elemental analysis, which is the disadvantage of having to analyze the existing elemental analysis and proximate analysis separately. In the future, more correlation models should be developed in future studies to improve the model for lesser error.

Supplementary Materials: The following supporting information can be downloaded at: https://www.mdpi.com/article/10.3390/en16010509/s1, Table S1: Element and proximate analyses results for correlation.

Author Contributions: Conceptualization, S.P. and S.J.K.; methodology, S.P., S.J.K., and K.C.O.; software, S.P. and S.J.K.; validation, S.P., S.J.K., and L.H.C.; investigation, S.P. and S.J.K.; data curation, S.P., S.J.K., L.H.C. and D.K.; writing—original draft preparation, S.P. and S.J.K.; writing—review and editing, S.P., S.J.K. and D.K.; supervision, D.K.; funding acquisition, D.K. All authors have read and agreed to the published version of the manuscript.

Funding: This research was funded by the Basic Science Research Program through the NATIONAL RESEARCH FOUNDATION OF KOREA (NRF) funded by the MINISTRY OF EDUCATION (2021R1A6A1A0304424211) and was carried out with the support of "R&D Program for Forest Science Technology (Project No. "FTIS 2021352B10-2223-AC03")" provided by the KOREA FOREST SERVICE (Korea Forestry Promotion Institute).

Conflicts of Interest: The authors declare no conflict of interest.

References

1. Yi, L.; Feng, J.; Qin, Y.H.; Li, W.Y. Prediction of elemental composition of coal using proximate analysis. *Fuel* **2017**, *193*, 315–321. [CrossRef]
2. Ceylan, Z.; Sungur, B. Estimation of coal elemental composition from proximate analysis using machine learning techniques. *Energy Sources Part A Recover. Util. Environ. Eff.* **2020**, *42*, 2576–2592. [CrossRef]
3. Telmo, C.; Lousada, J.; Moreira, N. Proximate analysis, backwards stepwise regression between gross calorific value, ultimate and chemical analysis of wood. *Bioresour. Technol.* **2010**, *101*, 3808–3815. [CrossRef] [PubMed]
4. Shen, J.; Zhu, S.; Liu, X.; Zhang, H.; Tan, J. The prediction of elemental composition of biomass based on proximate analysis. *Energy Convers. Manag.* **2010**, *51*, 983–987. [CrossRef]
5. Qian, C.; Li, Q.; Zhang, Z.; Wang, X.; Hu, J.; Cao, W. Prediction of higher heating values of biochar from proximate and ultimate analysis. *Fuel* **2020**, *265*, 116925. [CrossRef]
6. Yin, C.-Y. Prediction of higher heating values of biomass from proximate and ultimate analys. *Fuel* **2011**, *90*, 1128–1132. [CrossRef]
7. Lawal, A.I.; Aladejare, A.E.; Onifade, M.; Bada, S.; Idris, M.A. Predictions of elemental composition of coal and biomass from their proximate analyses using ANFIS, ANN and MLR. *Int. J. Coal Sci. Technol.* **2021**, *8*, 124–140. [CrossRef]
8. Su, Y.; Zhang, S.; Liu, L.; Qi, P.; Xu, D.; Shi, L.; Gao, J.; Zhang, H.; Zhu, S. Upgrading biomass fuels via combination of CO_2-leaching and torrefaction. *Energy Fuels* **2021**, *35*, 5006–5014. [CrossRef]
9. Tu, R.; Jiang, E.; Yan, S.; Xu, X.; Rao, S. The pelletization and combustion properties of terrified Camellia shell via dry and hydrothermal torrefaction: A comparative evaluation. *Bioresour. Technol.* **2018**, *264*, 78–89. [CrossRef]
10. Cao, L.; Yuan, X.; Jiang, L.; Li, C.; Xiao, Z.; Huang, Z.; Chen, X.; Zeng, G.; Li, H. Thermogravimetric characteristics and kinetics analysis of oil cake and torrefied biomass blends. *Fuel* **2016**, *175*, 129–136. [CrossRef]
11. Chen, D.; Cen, K.; Cao, X.; Li, Y.; Zhang, Y.; Ma, H. Restudy on torrefaction of corn stalk from the point of view of deoxygenation and decarbonization. *J. Anal. Appl. Pyrolysis* **2018**, *135*, 85–93. [CrossRef]
12. Bai, X.; Wang, G.; Wang, D.; Wang, Z.; He, C. Physical and chemical properties of non-treated and torrefied wheat straw grinds. In Proceedings of the American Society of Agricultural and Biological Engineers ASABE Annual International Meeting, Orlando, FL, USA, 17–20 July 2016; pp. 2–8. [CrossRef]
13. Sibiya, N.T.; Oboirien, B.; Lanzini, A.; Gandiglio, M.; Ferrero, D.; Papurello, D.; Bada, S.O. Effect of different pre-treatment methods on gasification properties of grass biomass. *Renew. Energy* **2021**, *170*, 875–883. [CrossRef]
14. Wu, J.; Wang, L.; Ma, H.; Zhou, J. Investigation of element migration characteristics and product properties during biomass pyrolysis: A case study of pine cones rich in nitrogen. *RSC Adv.* **2021**, *11*, 34795–34805. [CrossRef] [PubMed]
15. Tsai, W.T.; Liu, S.C.; Hsieh, C.H. Preparation and fuel properties of biochars from the pyrolysis of exhausted coffee residue. *J. Anal. Appl. Pyrolysis* **2012**, *93*, 63–67. [CrossRef]
16. Huang, C.W.; Li, Y.H.; Xiao, K.L.; Lasek, J. Cofiring characteristics of coal blended with torrefied Miscanthus biochar optimized with three Taguchi indexes. *Energy* **2019**, *172*, 566–579. [CrossRef]
17. Wang, Q.; Han, K.; Gao, J.; Li, H.; Lu, C. The pyrolysis of biomass briquettes: Effect of pyrolysis temperature and phosphorus additives on the quality and combustion of bio-char briquettes. *Fuel* **2017**, *199*, 488–496. [CrossRef]
18. Shen, X.; Wu, Y.; Xu, X.; Su, J.; He, Z.; Jiang, E.; Ren, Y.; Sun, Y. Torrefaction enhanced biomass chemical-looping gasification coupled with CO_2-splitting via half doped $LaFe_{0.5}M_{0.5}O_3$ perovskites. *SSRN Electron. J.* **2022**, *234*, 107314. [CrossRef]
19. Xing, X.; Fan, F.; Jiang, W. Characteristics of biochar pellets from corn straw under different pyrolysis temperatures. *R. Soc. Open Sci.* **2018**, *5*, 1–10. [CrossRef]
20. Wang, H.; Wang, X.; Cui, Y.; Xue, Z.; Ba, Y. Slow pyrolysis polygeneration of bamboo (Phyllostachys pubescens): Product yield prediction and biochar formation mechanism. *Bioresour. Technol.* **2018**, *263*, 444–449. [CrossRef]
21. Sharma, T.; Ratner, A. Analysis and characterization of metallic nodules on biochar from single-stage downdraft gasification. *Processes* **2021**, *9*, 533. [CrossRef]
22. Wu, C.; Budarin, V.L.; Wang, M.; Sharifi, V.; Gronnow, M.J.; Wu, Y.; Swithenbank, J.; Clark, J.H.; Williams, P.T. CO_2 gasification of bio-char derived from conventional and microwave pyrolysis. *Appl. Energy* **2015**, *157*, 533–539. [CrossRef]
23. Zhu, G.; Yang, L.; Gao, Y.; Xu, J.; Chen, H.; Zhu, Y.; Wang, Y.; Liao, C.; Lu, C.; Zhu, C. Characterization and pelletization of cotton stalk hydrochar from HTC and combustion kinetics of hydrochar pellets by TGA. *Fuel* **2019**, *244*, 479–491. [CrossRef]
24. Bian, R.; Ma, B.; Zhu, X.; Wang, W.; Li, L.; Joseph, S.; Liu, X.; Pan, G. Pyrolysis of crop residues in a mobile bench-scale pyrolyser: Product characterization and environmental performance. *J. Anal. Appl. Pyrolysis* **2016**, *119*, 52–59. [CrossRef]
25. Peng, J.; Bi, X.T.; Lim, C.J.; Peng, H.; Kim, C.S.; Jia, D.; Zuo, H. Sawdust as an effective binder for making torrefied pellets. *Appl. Energy* **2015**, *157*, 491–498. [CrossRef]

26. Luo, H.; Bao, L.; Kong, L.; Sun, Y. Low temperature microwave-assisted pyrolysis of wood sawdust for phenolic rich compounds: Kinetics and dielectric properties analysis. *Bioresour. Technol.* **2017**, *238*, 109–115. [CrossRef] [PubMed]
27. Kong, L.; Tian, S.H.; Li, Z.; Luo, R.; Chen, D.; Tu, Y.T.; Xiong, Y. Conversion of recycled sawdust into high HHV and low NOx emission bio-char pellets using lignin and calcium hydroxide blended binders. *Renew. Energy* **2013**, *60*, 559–565. [CrossRef]
28. Felfli, F.F.; Luengo, C.A.; Suárez, J.A.; Beatón, P.A. Wood briquette torrefaction. *Energy Sustain. Dev.* **2005**, *9*, 19–22. [CrossRef]
29. Zhao, S.; Zhang, Y.; Su, Y. Experimental investigation of rice straw oxidative pyrolysis process in a hot-rod reactor. *J. Anal. Appl. Pyrolysis* **2019**, *142*, 104646. [CrossRef]
30. Tsai, W.T.; Lin, Y.Q.; Tsai, C.H.; Chung, M.H.; Chu, M.H.; Huang, H.J.; Jao, Y.H.; Yeh, S.I. Conversion of water caltrop husk into torrefied biomass by torrefaction. *Energy* **2020**, *195*, 116967. [CrossRef]
31. Park, S.; Lee, S.; Joo, S.; Cho, L.; Oh, K.; Lee, S.; Jeong, I.S.; Lee, C.G.; Hong, S.J.; Kim, S.J.; et al. Simulation & model validation of torrefaction process and analysis of the fuel properties for pepper stem. *New Renew. Energy* **2017**, *13*, 64–70. [CrossRef]
32. Park, S.; Kim, S.J.; Oh, K.C.; Cho, L.; Kim, M.J.; Jeong, I.S.; Lee, C.G.; Kim, D. Investigation of agro-byproduct pellet properties and improvement in pellet quality through mixing. *Energy* **2020**, *190*, 116380. [CrossRef]
33. Chen, D.; Zhou, J.; Zhang, Q.; Zhu, X.; Lu, Q. Upgrading of rice husk by torrefaction and its influence on the fuel properties. *BioResources* **2014**, *9*, 5893–5905. [CrossRef]
34. Sarker, T.R.; Azargohar, R.; Dalai, A.K.; Meda, V. Enhancement of fuel and physicochemical properties of canola residues via microwave torrefaction. *Energy Rep.* **2021**, *7*, 6338–6353. [CrossRef]
35. Crombie, K.; Mašek, O.; Sohi, S.P.; Brownsort, P.; Cross, A. The effect of pyrolysis conditions on biochar stability as determined by three methods. *GCB Bioenergy* **2013**, *5*, 122–131. [CrossRef]
36. Adilah, S.; Nur, S.; Nurhayati, A. Slow pyrolysis of oil palm empty fruit bunches for biochar production and characterisation. *J. Phys. Sci.* **2014**, *25*, 97–112.
37. Ścisłowska, M.; Włodarczyk, R.; Kobyłecki, R.; Bis, Z. Biochar to improve the quality and productivity of soils. *J. Ecol. Eng.* **2015**, *16*, 31–35. [CrossRef]
38. Angin, D.; Şensöz, S. Effect of pyrolysis temperature on chemical and surface properties of biochar of rapeseed (Brassica napus L.). *Int. J. Phytoremed.* **2014**, *16*, 684–693. [CrossRef]
39. Matali, S.; Rahman, N.A.; Idris, S.S.; Yaacob, N.; Alias, A.B. Lignocellulosic biomass solid fuel properties enhancement via torrefaction. *Procedia Eng.* **2016**, *148*, 671–678. [CrossRef]
40. Sukiran, M.A.; Kheang, L.S.; Bakar, N.A.; May, C.Y. Production and characterization of bio-char from the pyrolysis of empty fruit bunches. *Am. J. Appl. Sci.* **2011**, *8*, 984–988. [CrossRef]
41. Ohliger, A.; Förster, M.; Kneer, R. Torrefaction of beechwood: A parametric study including heat of reaction and grindability. *Fuel* **2013**, *104*, 607–613. [CrossRef]
42. Ameen, A.; Saeed, H.; Harun, N.Y.; Nasef, M.M. Physicochemical characterization of different agricultural residues in Malaysia for bio char production. *Int. J. Civ. Eng. Technol.* **2019**, *2*, 10–22.
43. Chen, W.H.; Lu, K.M.; Tsai, C.M. An experimental analysis on property and structure variations of agricultural wastes undergoing torrefaction. *Appl. Energy* **2012**, *100*, 318–325. [CrossRef]
44. Rousset, P.; Aguiar, C.; Labbé, N.; Commandré, J.M. Enhancing the combustible properties of bamboo by torrefaction. *Bioresour. Technol.* **2011**, *102*, 8225–8231. [CrossRef]
45. Iáñez-Rodríguez, I.; Martín-Lara, M.Á.; Blázquez, G.; Pérez, A.; Calero, M. Effect of torrefaction conditions on greenhouse crop residue: Optimization of conditions to upgrade solid characteristics. *Bioresour. Technol.* **2017**, *244*, 741–749. [CrossRef] [PubMed]
46. Kim, S.J.; Oh, K.C.; Park, S.Y.; Ju, Y.M.; Cho, L.H.; Lee, C.G.; Kim, M.-J.; Jeong, I.-S.; Kim, D.-H. Development and validation of mass reduction prediction model and analysis of fuel properties for agro-byproduct torrefaction. *Energies* **2021**, *14*, 6125. [CrossRef]
47. Chen, W.H.; Huang, M.Y.; Chang, J.S.; Chen, C.Y.; Lee, W.J. An energy analysis of torrefaction for upgrading microalga residue as a solid fuel. *Bioresour. Technol.* **2015**, *185*, 285–293. [CrossRef] [PubMed]
48. Ministry of Environment. *Quality Test and Analysis Method of Solid Fuel Product*; Ministry of Environment: Seoul, Republic of Korea, 2014.
49. *ISO 18134-1*; 2015 Solid Biofuels—Determination of Moisture Content—Oven Dry Method—Part 1: Total Moisture—Reference Method. International Organization for Standardization: Geneva, Switzerland, 2015.
50. *ISO 18123*; 2015 Solid Biofuels—Determination of the Content of Volatile Matter. International Organization for Standardization: Geneva, Switzerland, 2015.
51. *ISO 18122*; 2015 Solid Biofuels—Determination of Ash Content. International Organization for Standardization: Geneva, Switzerland, 2015.
52. Jung, J.-M.; Park, S.-H.; Lee, Y.-S.; Gim, J.-H. The development of iInfrared thermal imaging safety diagnosis system using Pearson's correlation coefficient. *J. Korean Sol. Energy Soc.* **2019**, *39*, 55–65. [CrossRef]
53. Nhuchhen, D.R.; Abdul Salam, P. Estimation of higher heating value of biomass from proximate analysis: A new approach. *Fuel* **2012**, *99*, 55–63. [CrossRef]
54. Channiwala, S.A.; Parikh, P.P. A unified correlation for estimating HHV of solid, liquid and gaseous fuels. *Fuel* **2002**, *81*, 1051–1063. [CrossRef]

55. Oh, K.C.; Kim, J.; Park, S.Y.; Kim, S.J.; Cho, L.H.; Lee, C.G.; Roh, J.; Kim, D.H. Development and validation of torrefaction optimization model applied element content prediction of biomass. *Energy* **2021**, *214*, 119027. [CrossRef]
56. Shao, J.; Cheng, W.; Zhu, Y.; Yang, W.; Fan, J.; Liu, H.; Yang, H.; Chen, H. Effects of combined torrefaction and pelletization on particulate matter emission from biomass pellet combustion. *Energy Fuels* **2019**, *33*, 8777–8785. [CrossRef]
57. Pentananunt, R.; Rahman, A.N.M.M.; Bhattacharya, S.C. Upgrading of biomass by means of torrefaction. *Energy* **1990**, *15*, 1175–1179. [CrossRef]
58. Couhert, C.; Salvador, S.; Commandré, J.M. Impact of torrefaction on syngas production from wood. *Fuel* **2009**, *88*, 2286–2290. [CrossRef]
59. Suman, S.; Gautam, S. Pyrolysis of coconut husk biomass: Analysis of its biochar properties. *Energy Sources Part A Recover. Util. Environ. Eff.* **2017**, *39*, 761–767. [CrossRef]
60. Zhao, S.X.; Ta, N.; Wang, X.D. Effect of temperature on the structural and physicochemical properties of biochar with apple tree branches as feedstock material. *Energies* **2017**, *10*, 1293. [CrossRef]
61. Karaosmanoğlu, F.; Işigigür-Ergüdenler, A.; Sever, A. Biochar from the straw-stalk of rapeseed plant. *Energy Fuels* **2000**, *14*, 336–339. [CrossRef]
62. Wallace, C.A.; Afzal, M.T.; Saha, G.C. Effect of feedstock and microwave pyrolysis temperature on physio-chemical and nano-scale mechanical properties of biochar. *Bioresour. Bioprocess.* **2019**, *6*, 33. [CrossRef]
63. Manatura, K. Inert torrefaction of sugarcane bagasse to improve its fuel properties. *Case Stud. Therm. Eng.* **2020**, *19*, 100623. [CrossRef]
64. Xie, R.; Zhu, Y.; Zhang, H.; Zhang, P.; Han, L. Effects and mechanism of pyrolysis temperature on physicochemical properties of corn stalk pellet biochar based on combined characterization approach of microcomputed tomography and chemical analysis. *Bioresour. Technol.* **2021**, *329*, 124907. [CrossRef] [PubMed]